Continuous Modeling Technique of Fiber Pullout from a Cement Matrix with Different Interface Mechanical Properties Using Finite Element Program

Abstract

Fiber-matrix interface performance has a great influence on the mechanical properties of fiber reinforced composite. This influence is mainly presented during fiber pullout from the matrix. As fiber pullout process consists of fiber debonding stage and pullout stage which involve complex contact problem, numerical modeling is a best way to investigate the interface influence. Although many numerical research works have been conducted, practical and effective technique suitable for continuous modeling of fiber pullout process is still scarce. The reason is in that numerical divergence frequently happens, leading to the modeling interruption. By interacting the popular finite element program ANSYS with the MATLAB, we proposed continuous modeling technique and realized modeling of fiber pullout from cement matrix with desired interface mechanical performance. For debonding process, we used interface elements with cohesive surface traction and exponential failure behavior. For pullout process, we switched interface elements to spring elements with variable stiffness, which is related to the interface shear stress as a function of the interface slip displacement. For both processes, the results obtained are very good in comparison with other numerical or analytical models and experimental tests. We suggest using the present technique to model toughening achieved by randomly distributed fibers.

Keywords

Modeling of fiber, pullout, fiber-matrix interface model, finite element method, variable stiffness spring element.

Leandro Ferreira Friedrich [a]
Chong Wang [a]

[a] Applied Mechanics Group, Graduate Program in Engineering, Federal University of Pampa, Alegrete, RS, Brazil.
leandroffriedrich@gmail.com
wangchong@unipampa.edu.br

1 INTRODUCTION

It is well known that tensile strength of the brittle material, such as concrete, ceramic and glass, is much lower than its compressive strength. However, the addition of fibers into the brittle matrix

can significantly increase the material fracture strength. We can rate the main advantages of fiber reinforcement composites with the brittle matrix as (1) improvement in fracture toughness and tensile strength of the composite and (2) inhibition of crack-open and propagation. These desirable features have been obtained with a low fiber volume fraction, generally less than 2% (Fantilli and Vallini, 2008).

The fiber-matrix interface property directly affects the mechanical behavior of the composite. The most common way to observe the interface effect is through fiber pullout tests, which consists of debonding process and followed pullout process (Figure 1). For these two processes, the adhesion between fiber and matrix is the key (Kim and Mai, 1998). Engineers and researchers always seek for new techniques of characterizing interface and numerical methods to determine the strengths of the composite reinforced by the fibers with the characterized interface in order to obtain better composites with expected mechanical performance. For this, a number of numerical and computational models has been developed.
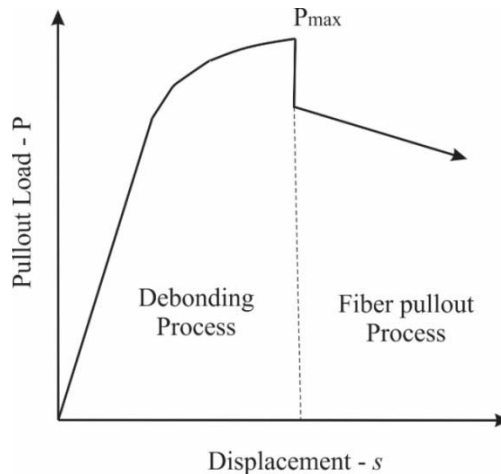

Figure 1: Typical fiber pullout test curve.

Without a doubt, the finite element method is one of the best computational tools to solve this problem. With a focus on local mixed-mode at the interface, Becker and Lauke (1997) developed a finite element model using a fracture mechanics criterion for the interface debonding process of a single fiber pullout test. Also using this kind of test, Liu et al. (1999) investigated the effects of fiber pullout rate, thermal residual stress, friction coefficient and fiber volume fraction. In their work, the local shear strain criterion was adopted for interface debonding. Recently, Wei et al. (2012) implemented a cohesive damage model in finite element modeling to simulate fiber-matrix interface debonding in order to investigate the interface shear stress distribution and effects of shear stress transfer across the debonding interface. Pochiraju et al. (2001), Zhang X. et al. (2004) and Tsai et al. (2005) simulated fibers pullout from an epoxy matrix by the finite element method using interface and contact elements, the cohesive zone model and Coulomb friction. Rodrigues et al. (2015) used interface finite elements with high aspect ratio and modeled the interaction between the steel bars and concrete.

Since many parameters are involved in the pullout process such as the mechanical properties of fiber, matrix, and interface, as well as the geometry of the fiber (Wang and Friedrich, 2013), it is still difficult to continuously model a single fiber pullout test. Others factors such as mesh and contact problems increase the difficulty. Although the modeling of fiber pullout problem has been studied for almost twenty years, we note that the reports on the research advance are decreased substantially recently. The reason would rather be attributed to the great difficulty in the numerical convergence of modeling than that the problem has been resolved. Also, we note that there is scarcely the numerical modeling that can systematically deal with whole fiber pullout process with desired interface mechanical properties. No one of the reported works can continuously model whole fiber pullout with desired interface mechanical properties without interrupting and modifying the modeling program.

This work presents continuously modeling technique without interruption to simulate the whole process of fiber pullout from cement matrix using popular finite elements program ANSYS® interacting with the MatLab®. At debonding stage, we suggest using interface elements with the cohesive zone model (CZM) presented by Xu and Needleman (1994) and obtain a satisfied relationship between the tractions acting on the fiber surface and the displacements jump across the interface. At fiber pullout stage, we propose employing nonlinear spring elements to model the debonded interface. The nonlinear spring elements are of variable stiffness and able to relate interface shear behavior with fiber slip displacement relative to the matrix. The number of the nonlinear spring elements on the interface decreases with the fiber slip displacement. The switching from debonding process to pullout process is made automatically through a computational subroutine implemented in the software MatLab®.

2 PROPOSED FINITE ELEMENT MODEL FOR FIBER PULL-OUT PROCESS

The axisymmetric model representing a single fiber inserted in a concentric cylindrical matrix is shown in Figure 2. By use of the software ANSYS, all geometric models of fiber and matrix used in this work were discretized with 2700 elements named as PLANE182 by ANSYS. The element PLANE182 is defined by four nodes and each node has two degrees of freedom: translations in the nodal x and y directions. The element has plasticity, stress stiffening, large deflection, and large strain capabilities. To simulate different processes, two interface modes were used (Figure 2): interface elements for debonding process and spring elements for pullout process. For the interface element, the nodes on both sides (fiber and matrix) were duplicated. 300 asymmetric elements were used to represent the cohesive interface, each with 4 nodes and zero thickness. The interface element INTER202 of ANSYS has four nodes and two degrees of freedom at each node. The spring element COMBIN40 of ANSYS with nonlinear stiffness k is made up of a pair of nodes. One of them is on the fiber and another in the matrix. In total 150 spring elements were used. The COMBIN40 element has two nodes and is a combination of a spring-slider and damper in parallel, coupled to a gap in series. A mass may be associated with one or both nodal points. The element has one degree of freedom at each node, either a nodal translation, rotation, pressure or temperature.
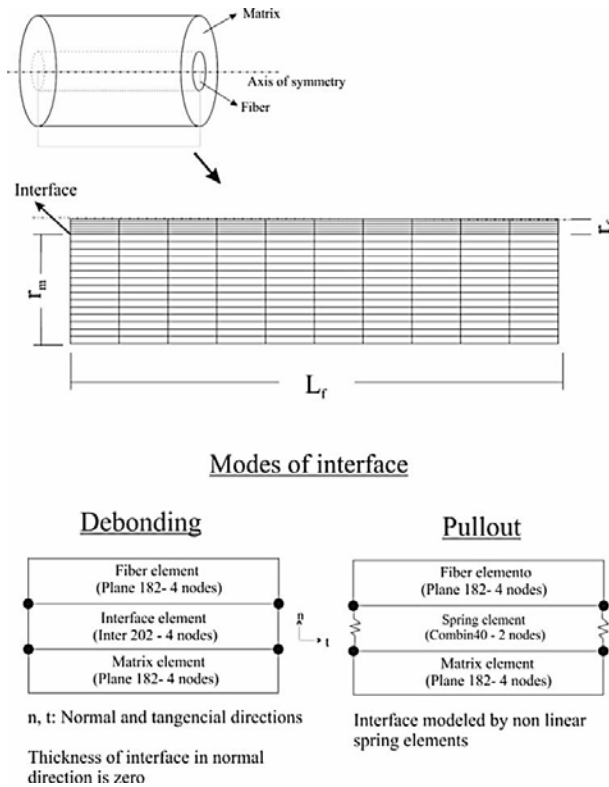
Figure 2: Axisymmetric concentric-cylinder model, mesh, and modes of the interface.

The debonding process is uniquely dependent on the required properties of the cohesive interface; meanwhile, the pullout process is dependent on the spring stiffness. When considering shear stress as constant, known as constant-τ model (Marshall et al. 1985, Gopalaratman and Shah 1987, Li 1992), we can write it as

$$\tau = \frac{P_{\max}}{\pi d L_e} \tag{1}$$

or

$$\pi d \tau = \frac{P_{\max}}{L_e} \tag{2}$$

where $P_{\max}$ is the maximal pullout load before the debonding process is over, d the fiber diameter and L_e the embedded length. If τ is constant, then the right term in Equation 2 is also constant. We denote the initial stiffness of the spring at the end of debonding process as

$$k_i = \pi d \tau = \frac{P_{\max}}{L_e} \tag{3}$$

which is corresponding the stiffness of the null slip displacement $s = 0$. When $s > 0$ we suggest the spring stiffness as:

$$k(s) = \frac{k_i(L_e - s)}{n(s)s}$$

(4)

where $n(s)$ is the number of effective springs. Using the spring stiffness determined in previous load step, we compute current slip displacement s and know the position of the fiber end node or how much nodes on the matrix side has been exceeded by the fiber end node, then, the number of effective springs can be accounted as the total nodes number on the matrix side minus the nodes number exceeded by the fiber end node (Figure 3). In this way, we can get the springs stiffness, k_i, for the next load step through Equation 4.
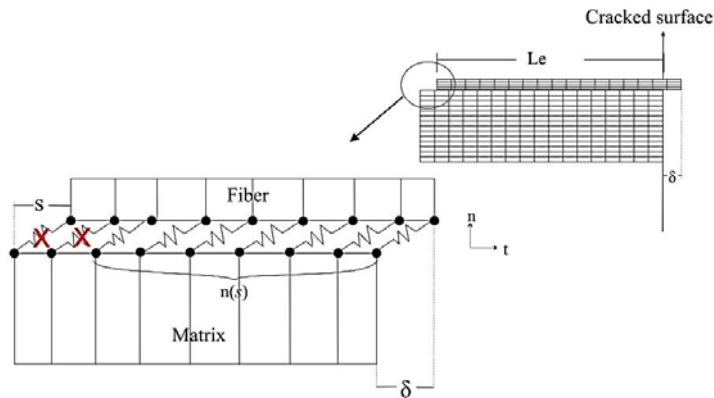

Figure 3: Determination of Effective springs.

However, the constant τ model is not suitable to describe the fiber pullout, since there is ample evidence which shows that the shear stress varies with the interface slip displacement and causes slip-hardening or slip-softening (Figure 4) as reported by Li and Stang (1997), Lin and Li (1997) and Wang et al. (1988). The variation may be attributed to several factors such as fiber surface abrasion, interface roughness, matrix plasticity, fragmentation of fibers coatings at the interface, etc.
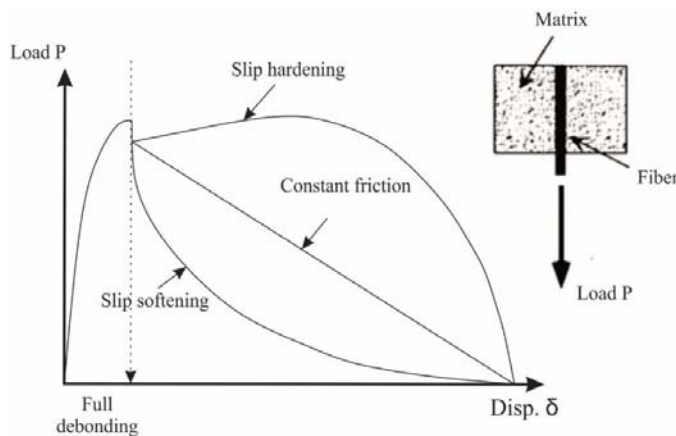

Figure 4: Three typical profiles of single fiber pullout curve Kang et al. (2000).

In these cases, the spring stiffness is also a function of the variation of the shear stress and thus, we propose the spring stiffness as

$$k(s) = \frac{\tau(s)\pi d(L_e - s)}{n(s)s} \tag{5}$$

Using this relation, we can simulate the pullout of fibers in different types, for example, steel fiber with slip softening behavior, as seen in the experimental works of Naaman and Shah (1976) and Li et al. (1991) and synthetic fibers with slip hardening behavior commonly observed in this fiber type, where the interfacial stress increases with slip distance (Wang et al. (1988), Li et al. (1995) and Ting et al. (2015)). This hardening behavior is due to wear between the surfaces, occurring at the moment when low hardness fibers try to slide over the stiffer matrix, a resistance to movement is imposed by the accumulation of the fiber debris, and thus increases the interface shear stress. These characteristics bring us a comprehensive model for simulating a great number of cases and helping to evaluate others factors such as fiber bridging stress and toughening.

3   COMPUTER ANALYSIS PROCEDURE

The MATLAB is a powerful program that offers not only different optimization algorithms already implemented but also the possibility of conducting an optimization algorithm defined by the user. Thus, the interactive use of the MATLAB and the ANSYS allows the user to fully control and optimize the simulation in order to get the best results as soon as possible.

Figure 5 shows the computational procedure made in this work. We performed simulations using the commercial software ANSYS® 11.0. With the aid of MATLAB® R2012a software, we shortened the simulation time and facilitated switching between debonding and pullout processes and taking the loop of the displacement δ applied at the right end of the fiber (Figure 3).

Following the procedure, first, we start the subroutine *pullout.m* in Matlab and create the text file "debonding.txt" by introducing an initial small displacement δ about 0.01 mm. The *txt* file contains the commands in *ANSYS Parametric Design Language* (APDL), which generate the geometric model, mesh and displacement restrictions of the model and finite element solution in batch mode. The displacement restrictions are imposed on the boundary of matrix cylinder.

As a result, the ANSYS yields the file "*Results.txt*" in two columns: the first for the applied displacement δ and the second for the reaction force obtained as the sum of the reactions at the displacement prescript nodes. If debonding is over, the reaction force will drop to zero. Therefore, after the computation of current load is accomplished, we check whether the reactions sum is zero in order to verify whether debonding has been finished. If not yet, we increase the displacement by an amount same as the initial displacement applied. The new results are stored as a new line in the "*Results.txt*" file.

If the condition of zero reactions sum is met, i.e. the debonding has been completed, the subroutine loads the new file "*Pullout.txt*", and then the interface elements are switched to spring elements and the characterized behavior of shear stress on the interface is introduced. Start again with the displacement δ applied and the initial stiffness k_i both obtained immediately before the debonding completion and calculate the displacement of the left end of the fiber, which is sliding relatively to the matrix i.e. the slip displacement *s*. The sliding quantity determines the number of effective

springs $n(s)$ as shown in Equations 4 or 5 and alters the spring stiffness, depended on what shear stress behavior is expected. Following this, a new larger displacement δ is added. The modeling is kept on until no effective spring is available, which means that the pullout process is over.
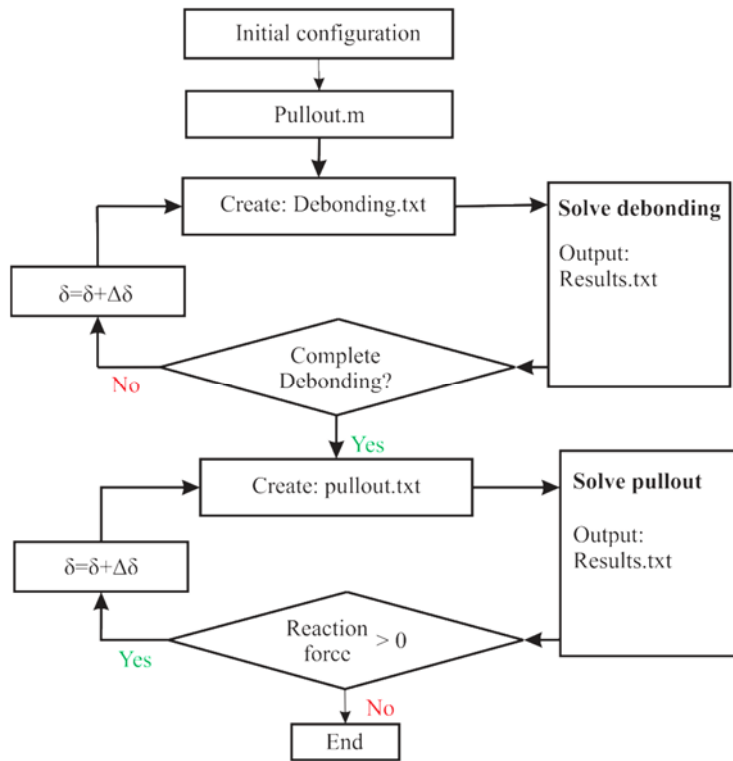

Figure 5: Computational procedure for fiber pullout.

4 RESULTS AND DISCUSSION

4.1 Debonding Process

The cohesive zone model consists of a constitutive relationship between tractions **T** acting on the interface and the corresponding separation distances i.e. displacement jump **Δ** across the interface (Lin et al. 2001). The use of cohesive zone allows a better control over the debonding process. As soon as the final separation is accomplished, the pullout process will start.

In the present work, the fiber-matrix interface was based on the exponential failure model of Xu and Needleman (1994) and the modeling was accomplished through commercial finite element software ANSYS 11.0 where for interface separation, only three parameters are needed: (1) maximum normal stress σ_{max} at the interface; (2) normal characteristic length δ_n and (3) tangential characteristic length δ_t .

The experimental test of Li et al. (1991) is generally used for the validation of the cohesive zone model of the debonding process. The authors Li et al. paid great attention to the process and their work has become a typical reference for the study on the behavior of steel fibers inserted into cement matrix. The geometric and mechanical properties of steel fiber and cement matrix, as well as

interface parameters used, are listed in Table 1. Since there is little information on the tested specimens, we assume that the matrix is 1.43 mm in diameter and 12 mm in length, approximately corresponding to fiber volume fraction 2%.

Fiber				Matrix			Interface debonding		
d_f	L_f	E_f	ν	f_c [a]	E_m	ν	σ_{max} [c]	δ_n [b]	δ_t [b]
(mm)	(mm)	(GPa)		(MPa)	(GPa)		(MPa)	(mm)	(mm)
0.204	12	210	0.3	36.5	34	0.2	2.54	0.012	0.12

[a] By experimental test from Leung and Shapiro (1999) where the elastic modulus was 30 GPa; [b]Estimate; [c]By Li and Mobasher (1998).

Table 1: Mechanical and geometrical properties of the specimen considered.

The matrix is characterized by the stress-strain curve in compression, as shown in Figure 6, with the maximum compressive strength equal f_c. We suggested a curve and implanted it into the ANSYS in order for the modeling to be more realistic.
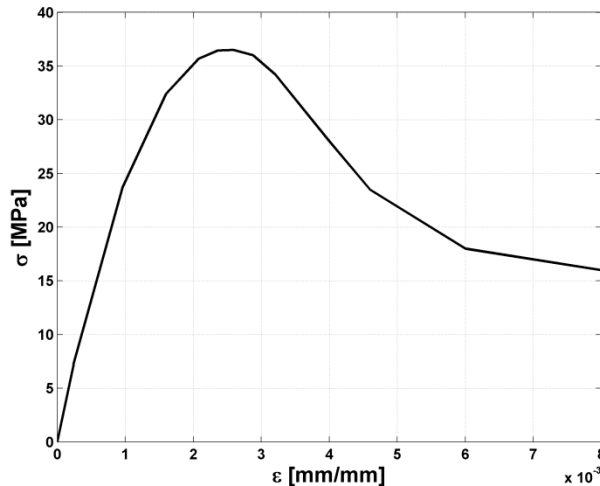

Figure 6: Stress-strain curve in compression suggested for the concrete.

The obtained results are compared with the experimental test of Li et al. (1991) and the two numerical models of Mobasher and Li (1995) and Li and Mobasher (1998) (Figure 7). These two numerical models dealt the interface in different manners. The first developed a theoretical model of interface failure based on the criterion of maximum strain energy release rate applied to a partially debonding length; meanwhile, the second dealt the interface as a third linear elastic phase of the composite, where the debonding criterion is given by integrating maximal normal and shear stresses into the finite element method.

From Figure 7 we see that the proposed model produces a good approximation to the experimental results, especially when the slip is large. Regardless of there is still a bit of deviation from the experiment curve on the initial debonding stage, in comparison with the other two numerical models, we get a better curve of pullout force - slip displacement, because the curves resulted from

the other numerical models can not extend to a sufficient slip displacement and the debonding process is ended too early. Furthermore, our pullout force peak appears at an instant closest to the experimental one. The maximal peak load obtained in the debonding process is a very important parameter for the pullout modeling, as shown in Equation 3, because it determines the initial spring stiffness that would compromise the results.
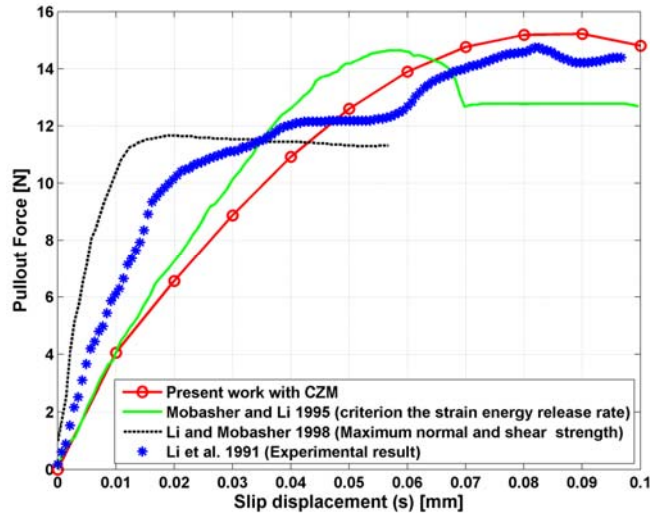

Figure 7: Comparison of pullout force *vs* slip displacement of present work, Mobasher and Li (1995), and Li and Mobasher (1998) with the experimental test of Li et al. (1991).

To check whether the slip displacement step size affects the pullout force, we repeated the computation and plot Figure 8 bellow with slip displacement in different step sizes. From Figure 8 we see that the slip displacement step size doesn't affect the pullout force. This coincides with our intuition that the slip displacement step size shouldn't influence the pullout force.
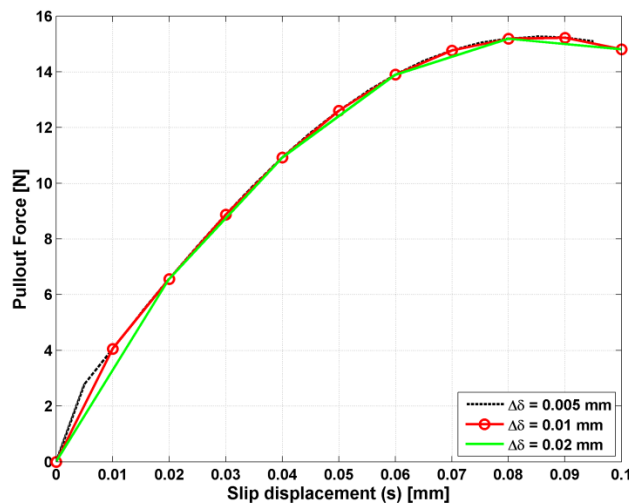

Figure 8: Influence of slip displacement step size $\Delta\delta$ on pullout force.

It has been verified that implanting the curve of stress-strain for concrete in compression into the ANSYS is indispensable. If the matrix phase is considered only as linear elastic, the results will be overestimated. Figure 9 shows the influence of three different concrete compressive curves on the pullout load. As observed, although the compressive curves are different, there is the unnoticeable difference in the responses obtained. It is not yet clear why there is little difference among the responses of the three compressive curves. Perhaps, the response is mainly depended on the interface performance parameters σ_{max}, δ_n (normal separation characteristic length) and δ_t (tangential separation characteristic length) as well as the matrix stiffness. However, there is an obvious difference between the response of linear elastic curve and the ones of the real compressive curves, which have the softening characteristic that inhabits continue raise of pullout load after the peak load reaches P_{max}. The curve 2 with a lower residual strength after the peak stress presents a slightly lower response than the others do.
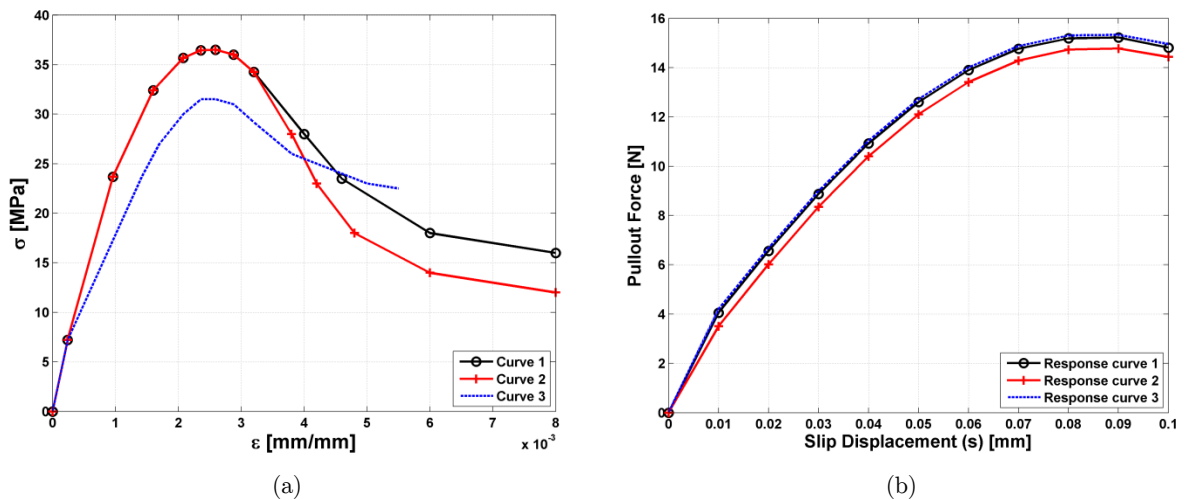

Figure 9: Influence of stress-strain compression curve of concrete on the pullout force.
(a) Different concrete compressive curves. (b) Responses of pullout force.

Figure 10 shows the influence of the interface strength (σ_{max}) during the debonding process. We note there is a significant increase in the maximum pullout force with increasing σ_{max}.

The gain in the pullout force is more than 100% when σ_{max} varies from 1.5 MPa to 3.5 MPa. The proper adhesion between fiber and matrix helps to enhance the composite strength. However if the adhesion is too strong to allow the fiber debonding, the stress in the fiber would exceed the fiber tensile strength and lead to the fiber breakage, decreasing the number of effective fibers, consequently, degrading contribution to improvement in the mechanical properties of the composite especially in the toughness, as demonstrated as some experiments reported by Li et al. (2001).
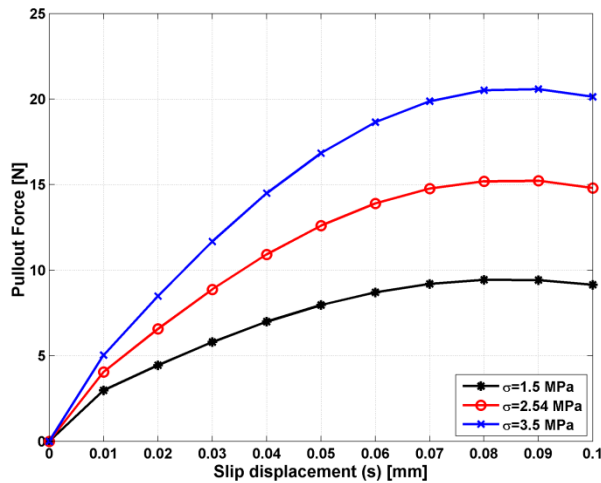
Figure 10: Influence of the interface strength σ_{max} with the interface characteristic parameters $\delta_t = 0.12mm$ and $\delta_n = 0.012mm$.

As the debonding predominantly occurred in the tangential direction, we also investigated the influence of tangential separation characteristic length δ_t on the pullout force. The curves of the pullout force *versus* slip displacement show an inverse relationship between the maximal pullout force and the interface characteristic length (Figure 11). This relationship may be attributed to the cohesive law of Xu and Needlemann (1994) used by the ANSYS, which imposes the conservation of the works realized by normal and tangential separations, resulting in the increase of shear stress and pullout force when the interface characteristic length decreases.
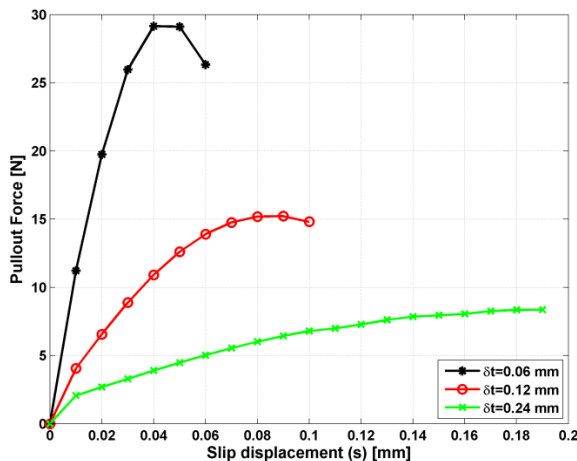

Figure 11: Influence of the tangential separation characteristic length δ_t, considering $\sigma_{max} = 2.54$ MPa for the interface normal strength.

4.2 Pullout Process

4.2.1 Slip Softening Modeling

As seen, the debonding process is represented very well by exponential failure model. Since the experimental test of Li et al. (1991) did not show the pullout process, thus, we validated the pullout model (Equation 4) by means of the experimental test of Leung and Shapiro (1999) who investigated the influence of steel fibers with different yield strengths (f_y). To simulate the slip softening behavior commonly observed in the composite reinforced by steel fibers, an appropriable interface shear stress model $\tau(s)$ should be introduced into the Equation 4.

In this work, after debonding process is accomplished, we adopted the relationship $\tau(s)$ suggested by Fantilli and Vanilli (2003) (Figure 12a) as:

$$\tau(s) = \tau_{fin} + (\tau_{max} - \tau_{fin})e^{k_c(s_1 - s)} \quad if \quad s > s_1 \tag{6}$$

where, τ_{max} is the maximum shear stress (Equation 1); s the slip displacement, which is approximately equal to δ the applied displacement; s_1 the applied displacement just immediately before debonding process was completed; τ_{fin} is the asymptotic value of shear stress and k_c a coefficient. These latter two parameters given in Figure 12b are dependent on fiber type and its manufacture process. There is the difference between the present work and of Fantilli and Vanilli in the determination of parameters s_1 and τ_{max}. Fantilli and Vanilli (2003) estimated s_1 and defined τ_{max} as function of fiber diameter and the concrete compressive strength. We got s_1 and τ_{max} in a more natural manner through simulating debonding process and identifying when the debonding process was over and the respectively applied displacement and maximal pullout force. It is clear that all these parameters rely on the CZM and the results obtained from the modeling of the debonding process, which is fundamental to complete the following modeling of fiber pullout process.
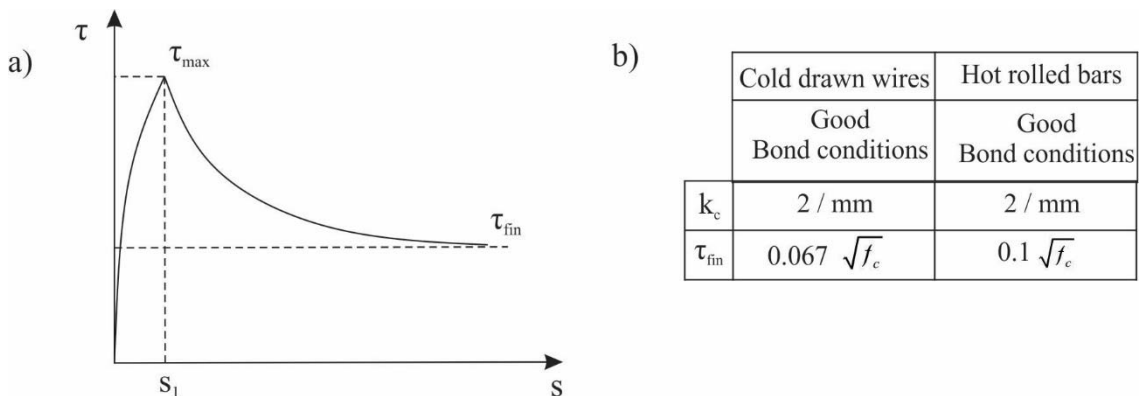

	Cold drawn wires	Hot rolled bars
	Good Bond conditions	Good Bond conditions
k_c	2 / mm	2 / mm
τ_{fin}	$0.067 \sqrt{f_c}$	$0.1 \sqrt{f_c}$

Figure 12: (a) Bond-slip relationship; (b) Bond parameters used by Fantilli and Vallini (2003).

Leung and Shapiro (1999) tested five specimen groups. For convenience, we simulated the case of the fiber type b. All parameters used are listed in Table 2, where f_t and f_c are the tensile and

compressive strengths of the matrix respectively. The required stress-strain relationship for concrete in compression is the same as in Figure 6, used for the debonding process validation. The composite has 0.05% of fiber volume fraction, which is defined here by the ratio of the volume of a single fiber to the matrix volume mentioned in section **4.1**.

Fiber				Matrix			Interface debonding		
d_f	L_f/L_e	E_f	ν_f	f_c^a	E_m	ν	σ_{max}^c	δ_n^b	δ_t^b
(mm)	(mm)	(GPa)		(MPa)	(GPa)		(MPa)	(mm)	(mm)
0.5	20/10	210	0.3	36.5	30	0.15	2.54	0.35	0.45

[a] By experimental test from Leung and Shapiro (1999) where the elastic modulus was 30 GPa; [b]Estimate; [c]By Li and Mobasher (1998).

Table 2: Mechanical and geometrical properties of the specimen by Leung and Shapiro (1999).

The comparison of results from the pullout process modeling is demonstrated in Figure 13. It is clear that the constant-τ model causes large discrepancies and the model of considering the interface shear as a function of the slip displacement, associated to maximum pullout load obtained in the debonding process, is more suitable for modeling pullout process. The model proposed in this work presents a good agreement with experimental result, especially when the slip displacement is larger than 2 mm. Therefore, the use of spring elements for simulating interface is able to control interface performance.

In comparison, our result and the analytical result of Fantilli and Vanilli (2007) are similar. With k_c=2 as used by Fantilli and Vanilli, our result prevails against the one of Fantilli and Vanilli only when the slip displacement is larger than 2 mm. However with k_c=5, our result is closer to the experiment curve over the whole pullout process.
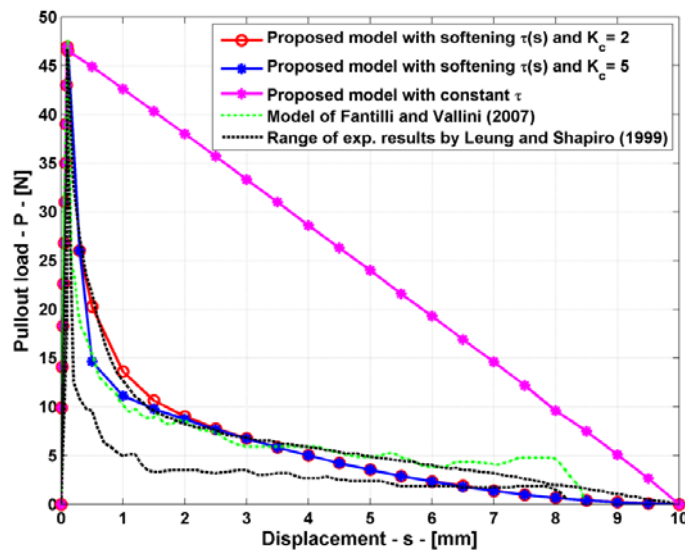

Figure 13: Comparison of the results from the proposed models, the analytical solution of Fantilli and Vallini (2007) and the experiment made by Leung and Shapiro (1999).

4.2.2 Slip Hardening Modeling

To exemplify interface slip hardening behavior we referred the experimental test of Li et al. (1995) where polyethylene fibers were added into a cement matrix. The geometric and mechanical properties of fiber, cement matrix, and interface parameters are listed in Table 3. The composite has 2% of fiber volume fraction.

Fiber				Matrix			Interface debonding		
d_f	L_f	E_f	ν_f	f_c^a	E_m	ν_m	σ_{max}^a	δ_n^a	δ_t^a
(mm)	(mm)	(GPa)		(MPa)	(GPa)		(MPa)	(mm)	(mm)
0.038	12	117	0.3	21	23	0.2	0.5	0.06	0.06

[a] Estimate.

Table 3: Mechanical and geometrical properties of the specimen considered.

For the comparison, the same experimental test was referred to the analytical model of Lin and Li (1997) with a simple interface constitutive relationship adopted from Bao and Song (1993) to quantify the slip-hardening interface behavior, which is:

$$\tau(s) = \tau_0 (1 - \beta s / d_f) \tag{7}$$

where the d_f is fiber diameter, τ_0 the frictional sliding shear stress at the tip of debonded zone where no slip occurs and β a dimensionless hardening parameter. The latter two parameters need to be determined empirically.

In terms of Equation 7, Lin and Li (1997) derived the pullout load:

$$P = \frac{\pi d_f^2 \tau_o (1+\eta)}{\omega} \left[\sinh\left(\frac{\omega L}{d_f}\right) - \sinh\left(\frac{\omega(s - s_o)}{d_f}\right) \right] + \pi \tau_o \beta (1+\eta)(s - s_o)(L - (s - s_o)) \tag{8}$$

where

$$\eta = \frac{V_f E_f}{V_m E_m}, \quad \omega = \sqrt{4(1+\eta)\beta \tau_o / E_f}, \quad s_o = \frac{2d_f}{\beta}\left[\cosh\left(\frac{\omega L}{d_f}\right) - 1\right] \tag{9}$$

This work adopted the slip hardening model created by Wang et al. (1998). The relationship between interface shear stress τ and slip displacement s in Equation 4 was taken as a quadratic function of s:

$$\tau(s) = a_0 + a_1 s + a_2 s^2 \tag{10}$$

where the constants a_0, a_1 and a_2 are empirically determined, so that the theoretical curves remain reasonably close to the experimental curves. We have chosen three load values to fit the experimental curve, they are P_1 (the load when the debonding was completed), P_2 (the maximal load of the experiment) and $P_3=0$ when the fiber was pulled out from the matrix.

Figure 14 gives the comparison of the results. Clearly, the proposed model produces an alike but better fiber pullout curve than the curves of Lin and Li (1997), who used an optimal parameter $\beta = 0.0125$, before the load hits its maximum. After the load attains the maximum, all the modeled curves deviate from the experimental curve, since the experimental curve is not quadratic. As seen, the β parameter is very sensible. To adequate value, many trials should be done. This is an uneasy matter. β with a value larger than 0.015 or less than 0.005 leads larger deviation from the experiment. With $\beta = 0.0125$, you get a good approximation to the experiment before the peak load but large deviation after then; with $\beta = 0.0085$, you have the inverse result. In comparison, our model has no need of trials but requires three load values. The first value is available automatically when the debonding is complete; the second value is fit to the maximal experimental one, and the third one is $P=0$ when the full fiber is pulled out from the matrix. Among the three values, only the second one is obligated to the experiment, the others are acquired naturally. With these three values, we got a better approximation to the experiment. Therefore, we can say that the presented model integrated into the ANSYS is suitable for the modeling because it is more simple but capable of describing very well the fiber pullout process.
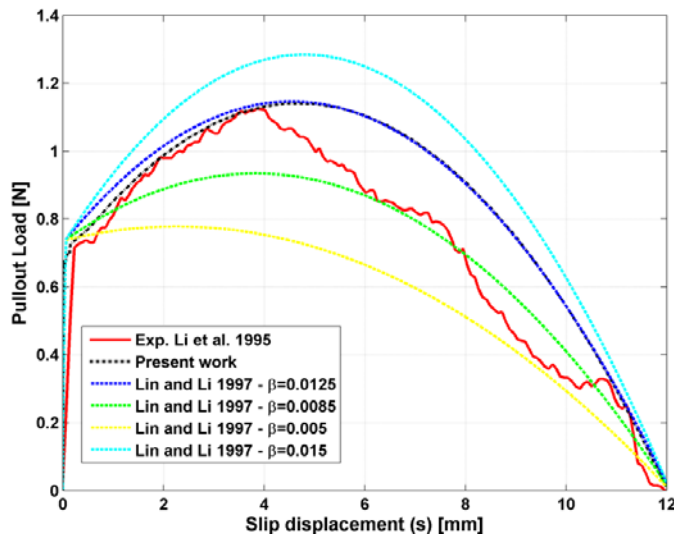

Figure 14: Comparison of results of the proposed model with the experimental test of Li et al. (1995) and the analytic model of Lin and Li (1997) with different β values.

5 REMARKS

As satisfactory results were obtained in the modeling, the following techniques are suggested to realize continuous modeling of fiber pullout process:

- For the debonding process, the employment of interface element with cohesive surface traction and exponential failure behavior is highly recommended.

- The compression test curve of the matrix material with a residual strength after peak load must be integrated into the modeling because linear elasticity behavior brings about super stiffness and leads modeling to fail.
- For pullout process, the use of spring elements with variable stiffness, which is associated to interface shear stress as a function of interface slip displacement through Equation 4 or 5 proposed in this work, prevails over contact elements and allows for modeling different interface shear behavior such as slip softening or hardening and constant shear.

Though we have realized the modeling by means of the ANSYS, the points given above may be included in any finite element programming for continuous modeling of fiber pullout process. The suggested computational procedure with the interaction of the ANSYS and the MATLAB can reduce substantially the time consumption in computation, which is of great advantage when there are a large number of parameters involved. With the presented technique, we are able to model toughening achieved by randomly distributed fibers.

Acknowledgement

References

Bao, G. and Song, Y., (1993). Crack bridging models for fiber composites with degraded interfaces, Journal Mechanical Physics and Solids 41: 1425-1444.

Beckert, W. and Lauke, B., (1997). Critical discussion of the single-fibre pull-out test: does it measure adhesion, Composites Science and Technology 57: 1689–1706.

Fantilli, A. P., and Vallini, P., (2003) A cohesive model for fiber-reinforced composites. In: Proceedings ISEC-02 Conference, Balkema, 1443–1449.

Fantilli, A. P., and Vallini, P., (2007). A cohesive interface model for the pullout of inclined steel fibers in cementitious matrices, Advanced Concrete Technology 5(2): 247–258.

Fantilli, A. P., Vallini, P., (2008). A cohesive interface model for the pullout of inclined steel fibers in cementitious matrices, Journal of Materials in Civil Engineering 20: 588-598.

Gopalaratnam, V. S., Shah, S. P., (1987) Tensile failure of steel fiber-reinforced mortar, Journal of Engineering Mechanics 113(5): 635-652.

Kanda, T., Lin, Z. and Li, V.C., (2000). Tensile stress-strain modeling of pseudo strain hardening cementitious composites, ASCE Journal of Materials in Civil Engineering 12(2): 147-156.

Kim, J.K. and Mai, Y.W., (1998). Engineered Interfaces in Fiber Reinforced Composites, Elsevier, Oxford.

Leung, C. K. Y. and Shapiro N., (1999). Optimal steel fiber strength for reinforcement of cementitious materials, Journal of Materials in Civil Engineering 112: 116–123.

Li, C.Y. and Mobasher B., (1998). Finite element simulations of fiber pullout toughening in fiber reinforced cement based composites, Advanced Cement Based Materials 7: 123-132.

Li, V. C. and Stang, H., (1997). Interface property characterization and strengthening mechanisms in fiber reinforced cement based composites, Advanced Cement Based Materials, 96-l.

Li, V. C., (1992). Post-crack scaling relations for fiber reinforced cementitious composites, ASCE Journal of Materials in Civil Engineering 4(l):41-57.

Li, V. C., Wang, S., and Wu, C., (2001). Tensile strain-hardening behavior of polyvinyl alcohol engineered cementitious composite (PVA-ECC), ACI Materials Journal 98(6): 483–492.

Li, V. C., Wu, H. C. and Chan, Y. W., (1995). Interfacial property tailoring for pseudo strain-hardening cementitious composites, In Advanced Technology on Design and Fabrication of Composite Materials and Structures 261-268.

Li, Z., Mobasher, B. and Shah, S. P, (1991). Characterization of interfacial properties of fiber reinforced cementitious composites, Journal of the American Ceramic Society 73(9): 2156-2164.

Lin, G., Geubelle. P.H. and Sottos. N.R., (2001). Simulation of fiber debonding with friction in a model composite pushout test, International journal of solids and structures 38: 8547-8562.

Lin, Z. and Li, V. C., (1997). Crack bridging in fiber reinforced cementitious composites with slip-hardening interfaces, Journal of the Mechanics and Physics of Solids 45(5): 763-787.

Liu, H.-Y., Zhang, X.Y, -W. Mai and X.-X. Diao, (1999). On steady-state fibre pull-out II. Computer simulation, Composites Science and Technology 59: 2191–2199.

Marshall, D.B., Cox, B.N. and Evans, A.G., (1985). The mechanics of matrix cracking in brittle matrix fiber composites, Acta Metall 33(11): 2013-2021.

Mobasher, B., and Li, C.Y., (1995). Modeling of stiffness degradation of the interfacial zone during fiber debonding, Composites Engineering 5(10-11): 1349-1365.

Naaman, A.E. and Shah, S.P., (1976). Pullout mechanisms in steel fiber reinforced concrete, Journal of structural engineering (ASCE) 102(8): 1537–1548.

Pochiraju, K.V., Tandom, G.P. and Pagano, N.J., (2001). Analyses of single fiber pushout consider interfacial friction and adhesion, Journal Mechanical Physics and Solids 49: 2307–2338.

Rodrigues, E.A., Manzoli, O.L., Bitencourt, L.A.G., Prazeres, P.G.C. and Bittencourt, T.N., (2015), Failure behavior modeling of slender reinforced concrete columns subjected to eccentric load, Latin American Journal of Solids and Structures 12: 520-541.

Ting, H., Zhang, Y. X., Su, Cheng. and Lo, S. R., (2015). Effect of Slip-Hardening Interface Behavior on Fiber Rupture and Crack Bridging in Fiber-Reinforced Cementitious Composites, Journal of engineering mechanics 1-14.

Tsai, J., Patra, A.K. and Wetherhold, R. (2005). Finite element simulation of shaped ductile fiber pullout using a mixed cohesive zone/friction interface model, Composites: Parte A 36: 827-838.

Wang C. and Friedrich L. F., (2013). Computational model of spalling and effective fibers on toughening in fiber reinforced composites at an early stage of crack formation, Latin American Journal of Solids and Structures 10: 797-811.

Wang Y., Li, V. C. and Backer S., (1988). Modeling of fiber pullout from a cement matrix. Composites, The international journal of cement composites and lightweight concrete 10(3): 143-149.

Wei, G. Liu, G. Xu, and C. X. Sun, (2012). Finite element simulation of perfect bonding for single fiber pull-out test, Advanced Materials Research 418–420: 509–512.

Xu, X.P. and Needleman, A., (1994). Numerical simulation of fast crack growth in brittle solids, Journal of the Mechanics and Physics of Solids 42: 1397–1434.

Zhang X., Liu H.Y. and Mai Y.W., (2004). Effects of fibre debonding and sliding on the fracture behavior of fibre-reinforced composites, Composites: Parte A 35: 1313-1323.